Hindawi
Advances in Civil Engineering
Volume 2022, Article ID 4879164, 13 pages
https://doi.org/10.1155/2022/4879164

Research Article

Nonlinear Finite Element Analysis and Comparison of In-Plane Strength of Circular and Parabolic Arched I-Section Cellular Steel Beam

Besukal Befikadu Zewudie

Faculty of Civil and Environmental Engineering, Jimma Institute of Technology, Jimma University, Jimma, Ethiopia

Correspondence should be addressed to Besukal Befikadu Zewudie; besubefk@gmail.com

Received 5 May 2022; Accepted 19 July 2022; Published 11 August 2022

Academic Editor: Nicola Buratti

The advancement in steel fabrication technology extends the structural and constructional advantages of cellular steel beams into arched cellular steel structure members. However, less attention is given to understanding the in-plane and out-of-plane structural behavior and performance of arched cellular steel beams. This article presents a numerical study using the finite element package ABAQUS to investigate the effect of arch axis geometry (circular and parabolic) and the impact of end support types on the in-plane inelastic buckling strength and buckling mode of I-section arched cellular steel beams. In the nonlinear finite element analysis of the model material nonlinearity, a second-order effect due to large deformation and initial geometric imperfection was incorporated in predicting inelastic buckling load and buckling mode. Furthermore, finite element analysis results were verified by comparing them to the existing experimental work. Test models covering shallow to deep arches of subtended angle in a range of 45–180 were investigated under uniformly distributed vertical loads and mid-span point loads. It was found that nonlinear finite element results fairly replicate the experimental work in predicting inelastic buckling load and post-buckling behavior. From the parametric investigation, it was found that deep parabolic arched cellular steel beams are structurally more efficient than their equivalent circular arched cellular steel beams. Pinned in-plane and free out-of-plane end support conditions result in a reduced inelastic ultimate buckling load capacity of arched cellular steel members when compared to other possible end support types. The geometry of an arch axis has no noticeable impact on the buckling mode of arched cellular steel beams.

1. Introduction

Nowadays, due to the evolution of steel structure fabrication technology advancement, various types of structural steel sections have been produced to improve the mechanical properties, construction advantages, and aesthetics of steel sections to satisfy the architectural and structural engineering requirements. I-section steel beams with repeating web openings of different shapes, such as castellated, cellular, and sinusoidal beams, are good examples of structural steel section improvements. Cellular steel beams are made of hot-rolled I-section profiles by flame cutting of the parent profile by cutting into two semicircular sections through the web of a common steel I-beam section. Once the two cuts are completed, the halves are then separated, shifted, and welded together to form a new, deeper, stiffer, stronger section [1, 2]. As a result of expanding the web depth and introducing web openings, cellular steel beam members have an increased depth-to-weight ratio, an increased section modulus, and increased strong-axis moment of inertia and allow running utilities through the openings when compared to its solid web parent profiles [1–3]. These structural and construction advantages extend the application of cellular steel beams in the form of arched structural members. Arched I-section cellular steel beams are the perfect solution for the long-span curved roof structures of buildings and bridges due to their weight-saving, elegance, and ability to integrate constructional utility advantages [1, 4]. Even though cellular steel beams have numerous advantages, the presence of repeated web opening introduces additional failure modes such as

Vierendeel, web post-buckling, and web post-fracture that are not expected in solid web I-section steel beam members [5]. Vierendeel yielding is among the local failure modes of cellular steel beams, which are identified as bending around the opening by forming four plastic hinges around the opening due to the high shear transfer mechanism around the opening. Experimental and numerical investigations by Panedpojaman et al. [6–9] carried out on the load-carrying capacity of steel beams with web openings on the Vierendeel failure mechanism and proposed an interaction relationship between axial force and moments, location of plastic hinge formation, and effective length of the opening to be considered in analyzing the Vierendeel bending resistance of steel beams with web openings. Another local failure mode associated with steel beams of repeating web openings is web post-buckling due to horizontal shear force passing through web post width, which induces compression stress on the web post between two openings, resulting in twisting of the web post over its vertical axis [10]. Several previous research [11–13] revealed web postfailure mode, identified determinant parameters that can affect web post-buckling, and developed novel design equations for web post-buckling resistance for both symmetric and asymmetric horizontal cellular and castellated steel beams. Rapture of welded joints sometimes occurs in castellated and cellular steel beams due to horizontal shearing force in the web post when there is inadequate web post length or a small length of the welded joint [2, 14]. In addition to the aforementioned local failure mode due to the slender cross-section over its parent profile, castellated and cellular steel beams are also susceptible to lateral-torsional buckling. Ferreira et al. [15] present the lateral-torsional resistance of cellular steel beams considering the load and resistance design factors to conclude that the design flexural strength was ineffective in the case of web postbuckling and lateral-torsional buckling occurring together. Recently, [16] investigated the effect of steel grade, cross-section dimension, and beam length on the ultimate strength and buckling mode of a castellated steel beam.

Nowadays, the application of cellular steel beams has extended to arched cellular steel beams because of improved mechanical structural behavior, constructional advantages, versatility, and aesthetics in achieving long spans. However, despite the structural and construction advantages of arched cellular steel beams, most of the previous analytical, numerical, and experimental investigations focused on the in-plane and out-of-plane structural behavior of solid web arched steel structures. Numerous research studies [17–22] reported on load-carrying capacity, buckling mode, effects of parameters like included angle, slenderness ratio, initial geometric imperfection, residual stress, and loading conditions on the inelastic in-plane and out-of-plane strength of circular and parabolic arched solid web steel arches with pinned and fixed-end supports.

Pi et al. [18] developed a lower-bound analyzing equation for the ultimate in-plane capacity of circular steel arches with hinged and fixed-end supports subjected to combined axial compressive and bending action. References [23, 24] studied the out-of-plane stability of pin-ended and fixed-ended freestanding circular arches of I-sections using a finite element method to analyze the out-of-plane inelastic flexural behavior of circular arches under uniform twist and uniform bending.

Gou et al. [25] experimentally investigated the magnitude and distribution of initial geometric imperfections' impact on the out-of-plane inelastic buckling strength of fixed-end arched steel members under symmetric and unsymmetrical loading conditions.

Despite several analytical, numerical, and experimental research on circular and parabolic arched solid web steel members, limited investigations were reported on the structural behavior of arched cellular steel beams. The work of Zaher et al. [26] is the only existing experimental investigation into the performance of arched cellular steel beams under mid-span point load, which comprises only four full-scale specimens with limited parameters. Also, Pandya and Dhankot [27] numerically studied the thermal variation effect on a curved castellated girder. From the above two related existing literature on an arched cellular steel beam, it is understandable that the inelastic in-plane structural strength and buckling mode of an arched cellular steel beam of different axis geometry under combined axial compression and bending moment with various end support configurations are not revealed. To seal this gap in theoretical understanding and to support further studies of the structural behavior of arched I-section cellular steel beams, there is a need to perform nonlinear finite element analysis on arched I-section cellular steel beams covering a wide range of parameters such as arch axis geometry, rise-to-span ratio, and different end support conditions. Therefore, this article presents a validated nonlinear finite element analysis of an arched cellular steel beam using the finite element program ABAQUS, considering the nonlinearity of material properties, a second-order effect due to large deflection, and initial geometric imperfection. Furthermore, parametric investigation on the impact of arch axis geometry and effect of end support type on elastic-plastic in-plane strength and buckling mode of arched I-section cellular steel with varying rise-to-span ratio under uniformly distributed vertical load and mid-span concentrated load cases was analyzed and interpreted.

2. Finite Element Modeling and Analysis

For modeling the three-dimensional geometry of arched cellular steel beams and analyzing buckling load, deflection, and postbuckling behavior of the test specimen's finite element program ABAQUS was used. Under this subsection, material properties, boundary conditions, finite element type and size, analysis steps, and finally validation of finite element analysis results were presented.

2.1. Material Properties. The elastic-plastic material properties used for this investigation were taken from an experimental tensile coupon test performed by Dou et al. [20]. The engineering bilinear stress-strain curve from the tensile coupon test result is given in Table 1 and Figure 1. In defining plastic material properties in FEA, engineering stress-

Table 1: Mechanical properties of the steel used for parametric investigation.

Plate origin	Plate thickness (mm)	Yield stress f_y (N/mm^2)	Modulus of elasticity E_s (MPa)	Ultimate stress f_u (N/mm^2)
Web	8	315	213×10^3	430
Flange	12	285	202×10^3	440

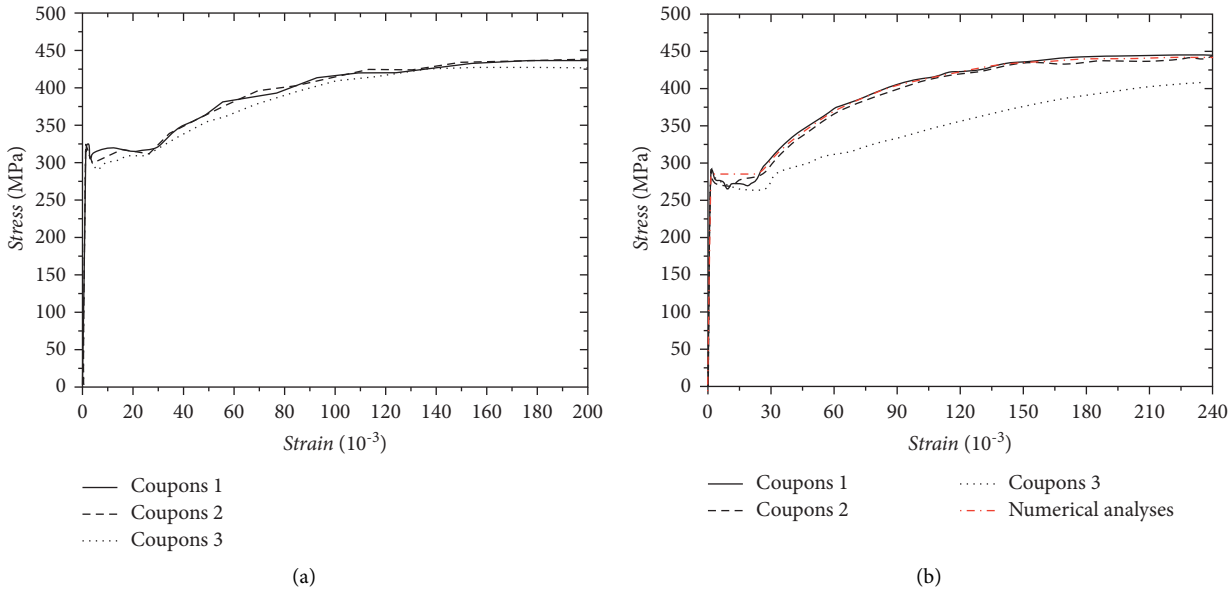

Figure 1: Bilinear stress-strain curve for (a) web and (b) flange [20].

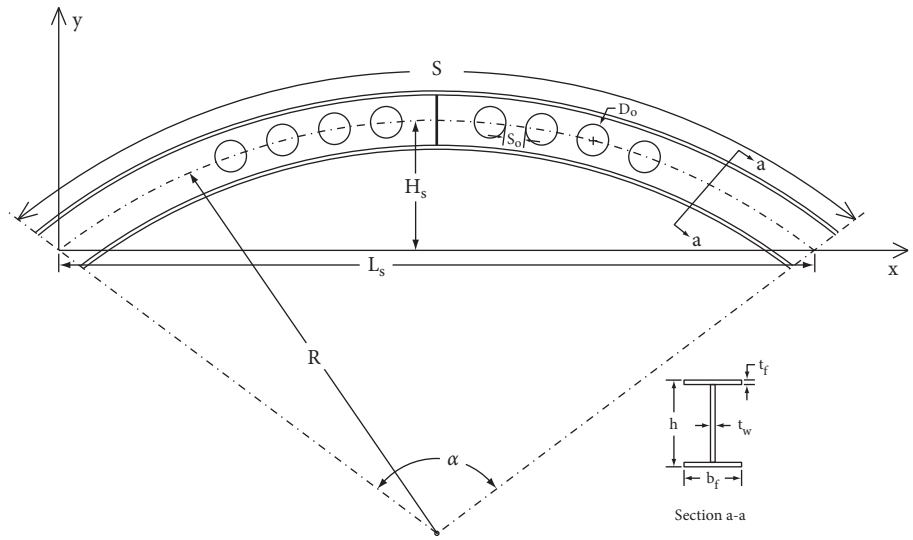

Figure 2: The geometry and the cross-sectional dimension of the test model.

strain results from tensile coupon tests are converted to true stress-strain relations for consideration of cross-sectional area change in the phase of testing using the equations given in [1, 2]. An elastic-plastic incremental stress-strain relationship derived from the von Mises yield criterion was utilized in this study:

$$\sigma_{\text{true}} = \sigma(1+\varepsilon),$$
$$\varepsilon^{pl}_{\text{true}} = \ln(1+\varepsilon) - \frac{\sigma_{\text{true}}}{E}. \quad (1)$$

2.2. Test Specimens. To investigate the elastic-plastic in-plane strength of circular and parabolic axis arched cellular steel beams, the class-1 I-section, which is capable of forming full plastic hinges, was selected based on the section that can be used for medium to high load-carrying capacity in actual engineering practice. The global and cross-sectional geometries of tested specimens are shown in Figure 2, where *Hs* is the arch rise, *S* is the arch length, *Ls* is the span length, *R* is the radius of the arch length, and α is the arch subtended angle. The cross-sectional dimensions of the cross-section are $h \times b_f \times t_w \times t_f = 250 \times 120 \times 8 \times 12mm$, where h is the

Table 2: Finite element test model database.

Specimen	(H_S/L_S)	α (deg)	R (mm)	H_S (mm)	Do (mm)	L_s (mm)	Load case-1	Load case-2
Circular axis arch geometry								
SCC-1	0.09	45	3280.3	247.5	160	2500	MSPL	UDVL
SCC-2	0.13	60	2515.8	332.5	160	2500	MSPL	UDVL
SCC-3	0.20	90	1768.4	517.5	160	2500	MSPL	UDVL
DCC-1	0.28	120	1457.9	707.5	160	2500	MSPL	UDVL
DCC-2	0.35	140	1330.3	875	160	2500	MSPL	UDVL
DCC-3	0.42	160	1269.5	1047.5	160	2500	MSPL	UDVL
DCC-4	0.5	180	1250	1250	160	2500	MSPL	UDVL
Specimen	(H_S/L_S)	R (mm)	H_S (mm)	Do (mm)	L_s (mm)	Load case-1	Load case-2	
Parabolic axis arch geometry								
PSC-1	0.09	3280.3	247.5	160	2500	MSPL	UDVL	
PSC-2	0.13	2515.8	332.5	160	2500	MSPL	UDVL	
PSC-3	0.20	1768.4	517.5	160	2500	MSPL	UDVL	
PDC-1	0.28	1457.9	707.5	160	2500	MSPL	UDVL	
PDC-2	0.35	1330.3	875	160	2500	MSPL	UDVL	
PDC-3	0.42	1269.5	1047.5	160	2500	MSPL	UDVL	
PDC-4	0.5	1250	1250	160	2500	MSPL	UDVL	

SCC: shallow circular curve, DCC: deep circular curve, PSC: shallow parabolic arch, PDC: deep parabolic arch, MSPL: mid-span point load, and UDVL: uniform distributed vertical load.

overall height, b_f is the flange width, t_w is the web thickness, and t_f is the flange thickness, respectively, as shown in Figure 2 section a-a. Web opening diameter (Do) and center-to-center spacing of the opening (S) along the centerline of arches were determined according to BS EN 1993-1-1 [28]. This standard recommends that the web opening diameter and web post length of cellular steel beams should be within the range given in equations (2) and (3) to avoid the formation of plastic hinges around the opening due to high shear stress concentration around the corner of the opening before occurrences of web post-buckling.

$$1.08 < \frac{S}{D_o} < 1.5, \tag{2}$$

$$1.25 < \frac{h}{D_o} < 1.75. \tag{3}$$

The opening diameter ($Do = 160$ mm), web post length ($S = 220$ mm), and web post width $S_0 = 60$ mm were used for this study based on the above criteria. The arch axis geometry of circular and parabolic arches was adopted from the American Institute of Steel Construction curved member design guide 33 [29]. Arch parameters like arch axis points (y), arch rise (Hs), rise-to-span ratio (H_S/L_S), and subtended angle (α) were computed using equations (5)–(7) for circular arch axis geometry. For the parabolic arch axis geometry, equation (7) was used. The geometrical parameters of the arch model specimens presented in Table 2 were sorted out according to the following relations:

$$y = H_S - R + \sqrt{R^2 - \left(\frac{Ls}{2} - x\right)^2}, \tag{4}$$

$$H_S = R\left[1 - \cos\left(\frac{\alpha}{2}\right)\right], \tag{5}$$

$$\frac{H_S}{L_S} = \frac{1 - \cos(\alpha/2)}{2\sin(\alpha/2)}, \tag{6}$$

$$y = 4H_S\frac{x}{L_S}\left(1 - \frac{x}{L_S}\right). \tag{7}$$

2.3. Finite Element Type and Mesh Size. The ABAQUS library provides shell elements that allow modeling of curved shells that can exhibit nonlinear material response and undergo large translation, rotation, and large strains [30]. In this investigation, a combined doubly curved thin shell element family of 4-node (S4R) and 3-node (S3R) linear geometric order with associated six degrees of freedom at each node and reduced integration numerical techniques were used to discretize the model. The accuracy of the FEA results and computational time required depend upon the size of mesh elements. The finer element size adds more nodes with a degree of freedom that can capture structural behavior accurately, but it requires longer computational time. On the contrary, the coarse element mesh size generates too few degrees of freedom in the model, which could result in an inaccurate analysis result in a very short period of solving time. So, it is important to iteratively decrease mesh element size from coarse to finer until analysis yields a converged solution. Beyond a certain element mesh size, the additional mesh refinement by decreasing element size has little or no effect on the analysis solution other than increasing solving time. For this study, a mesh element size of 20 mm typically discretizes the model into a shell element of 2,971 and with a number of nodes of 3,179 and gives converged results of eigenvalue, inelastic buckling load, and deflection of the model. Figure 3 shows the mesh model of test specimen SCC-2.

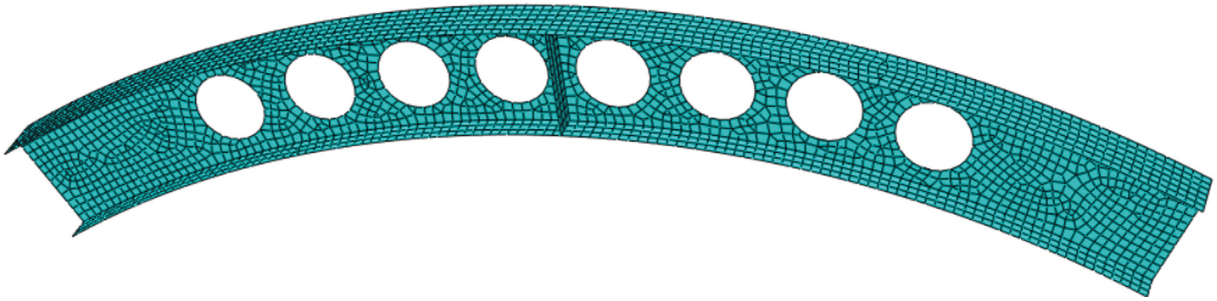

Figure 3: Finite element model mesh for SCC-2.

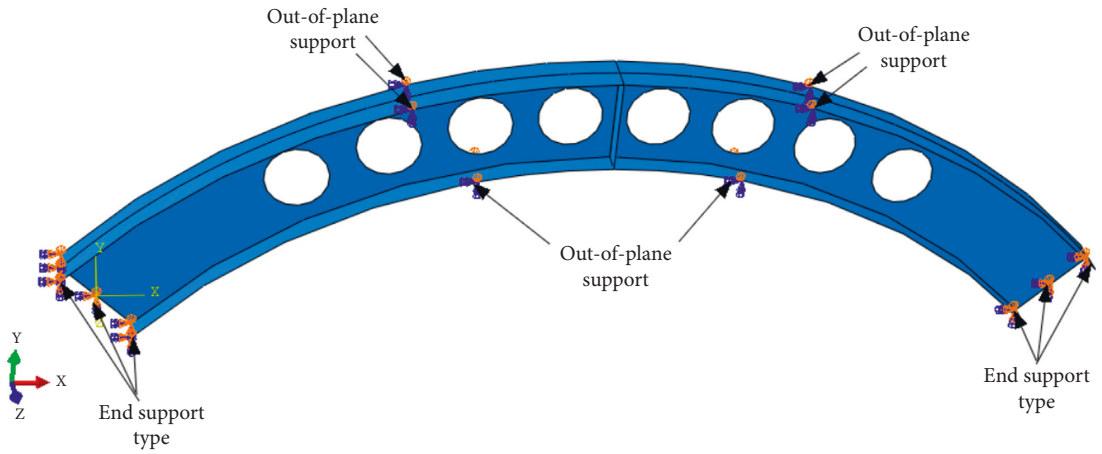

Figure 4: Boundary condition in finite element modeling.

Table 3: End support type used in the parametric investigation.

End support type		U_X	U_Y	U_z	θ_X	θ_Y	θ_Z
Pinned-free	Pinned in-plane, free out-of-plane	1	1	0	0	0	0
Pinned-pinned	Pinned in-plane, pinned out-of-plane	1	1	1	0	0	0
Fixed-pinned	Fixed in-plane, pinned out-of-plane	1	1	1	1	1	0
Fixed-fixed	Fixed in-plane, fixed out-of-plane	1	1	1	1	1	1
Out-of-plane support		0	0	1	1	1	0

1 = restrained, 0 = free, U = translation, and θ = rotation.

2.4. Boundary Condition and Loading. This study's prime focus was the in-plane inelastic buckling performance of arched cellular steel with postbuckling behavior to ensure this lateral support is provided at one-third of the span length to restrain premature out-of-plane buckling, as shown in Figure 4. Different possible end support conditions were considered in this investigation to understand the impact of end support type on buckling performance and buckling mode. A detailed description of the boundary conditions used for parametric investigation is given in Table 3. Web stiffeners are provided at mid-span under applied point load to avoid web crippling due to localized web yielding under the loading point.

2.5. Analysis Step. A two-step analysis procedure was incorporated for each model in this study to obtain the in-plane ultimate inelastic buckling load of an arched cellular steel beam with associated post-buckling behavior. First, linear buckling analyses were performed, considering only the linear behavior of material to extract eigenvalue using the subspace iteration method. From the extracted eigenvalue, the minimum eigenvalue with localized buckling mode was used as a reference elastic buckling load to extract the ultimate inelastic buckling load of the model in the second nonlinear analysis step. In general, in the second step, nonlinear analyses were performed by incorporating material nonlinearity behavior, initial geometric imperfection, and second-order effects due to large deflection (NLGEOM). The modified Riks algorithm method was used for nonlinear analysis. This method solves simultaneously for load and displacement, using the arc-length method of iteration procedure to trace the right equilibrium path for the nonlinear problems due to large geometry changes or material behavior in which softening and buckling instability dominate [31, 32].

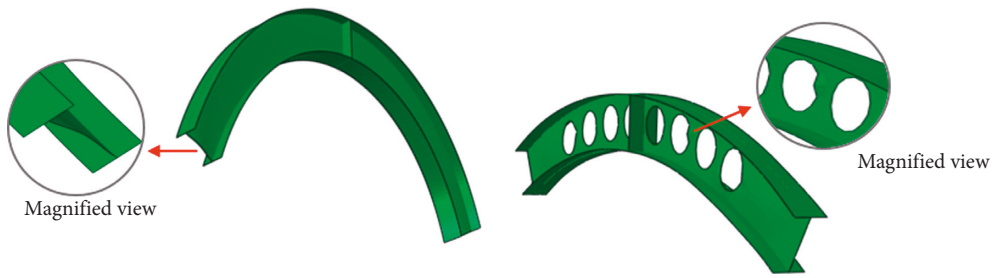

Figure 5: Model with initial geometric imperfection.

Table 4: Dimensional properties of experimentally tested arched cellular steel beam specimens by Zaher et al. [26].

Specimens	h (mm)	t_w (mm)	b_f (mm)	t_f (mm)	L_s (mm)	S (mm)	H_s (mm)	α (deg.)	Do (mm)	Yield stress, fy (MPa)		Ultimate stress, f_u (MPa)		Modulus of elasticity, Es (GPa)	
										Web	Flange	Web	Flange	Web	Flange
B-1	170	4	120	8	2451	2590	472	60	-	242	233	290	315	205	199
B-2	240	4	120	8	2451	2590	538	60	160	242	233	290	315	205	199
B-3	240	4	120	8	2651	2590	699	60	160	242	233	290	315	205	199
B-3	240	4	120	8	2032	2590	484	60	160	242	233	290	315	205	199

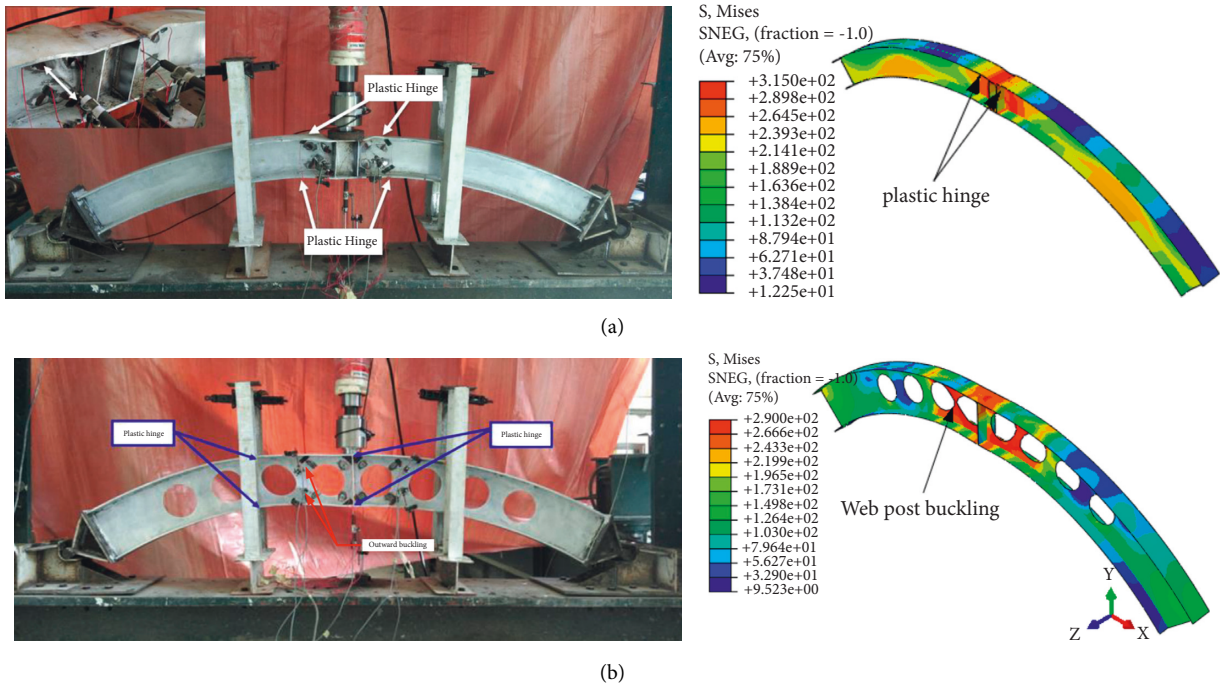

Figure 6: Experimental and FEA buckling mode comparison. (a) B-1 specimen buckling mode. (b) B-2 specimen buckling mode.

2.6. Initial Geometric Imperfection. In the process of cutting, bending to form an arch and transporting loss of straightness from an alignment is inevitable. This loss of straightness from an alignment (an initial geometric imperfection) has a significant impact on the initiation of buckling [25, 33]. Therefore, in finite element analysis, the superposition of the lowest eigenvalue local buckling mode obtained from linear buckling analysis with a scale factor of magnitude $S/1000$ provides a good estimation of the initial geometric imperfection of steel arches in the nonlinear analysis step [34], where S represents arch length, Figure 5 shows a magnified initial geometric imperfection of models B-1 and B-2.

2.7. Model Validation. To check the reliability of the finite element analysis results, an existing experimental research report by Zaher et al. [26] was used as a benchmark for FEA result validation. The cross-sectional dimension, arch geometry, and material properties of experimental specimens

Table 5: Comparative study on FE analysis result and experimental result.

Specimens	Ultimate buckling load (kN)				In-plane vertical deflection (mm)				Mode of buckling	
	P_{Exp}	P_{FEA}	P_{Exp}/P_{FEA}	Deviation (%)	U_{Exp}	U_{FEA}	U_{Exp}/U_{FEA}	Deviation (%)	FEA	EXP
B-1	253	259.9	0.97	2.67	44	52.6	0.84	16.34	Flexural bending	Flexural bending
B-2	124	120.7	1.02	2.36	24	20.11	1.19	16.20	Web postbuckling	Web postbuckling
B-3	137	126.7	1.08	7.52	18	20.58	0.87	14.33	Web postbuckling	Web postbuckling
B-4	130	130.3	0.99	0.23	17	19.28	0.88	13.41	Web postbuckling	Web postbuckling

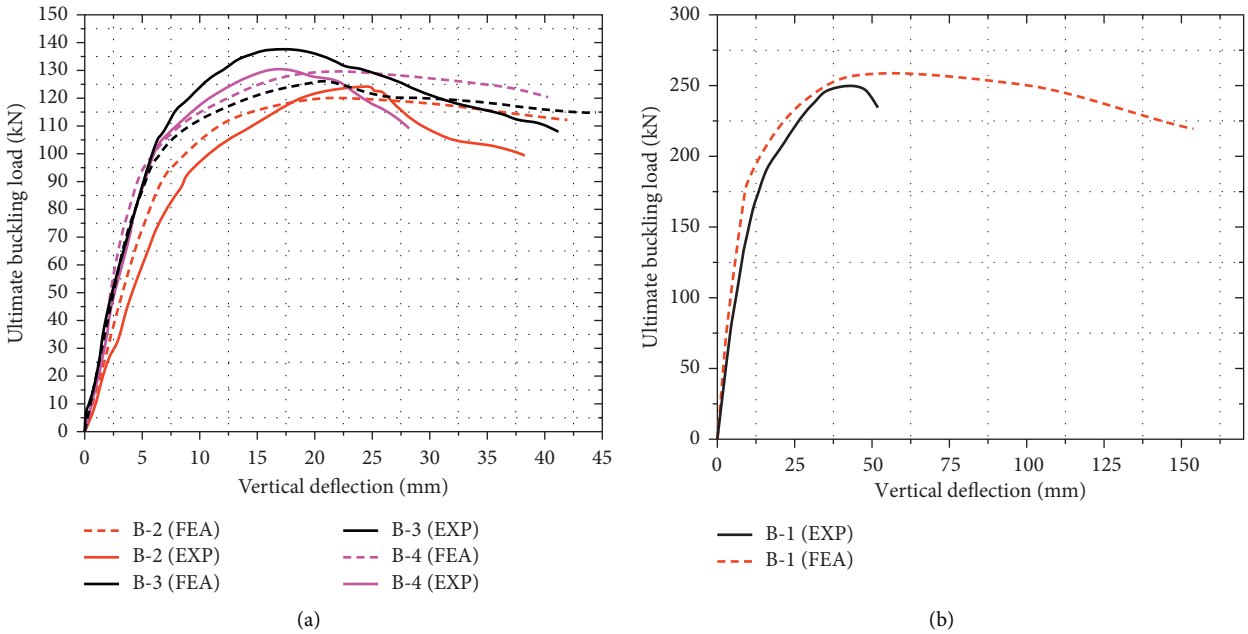

Figure 7: Load-deflection curve comparison of FEA and EX. (a) Arched cellular steel beam. (b) Solid web arched beam.

are described in Table 4. The graphical description of the symbol for arched cellular geometry used here is shown in Figure 2. The experimental test setup was as presented in Figure 6, but in this study, the fully pinned end support type was used in finite element modeling rather than the pivotal pin end support used in the experimental test model to account for real support conditions in engineering practices.

The ultimate inelastic buckling load versus in-plane vertical deflection at mid-span and the predicted post-buckling failure mode obtained from finite element analysis were compared to the existing experimental research results presented by [23]. From FEA simulation results, solid web test model B-1 fails in bending by forming plastic hinges in the vicinity of the applied load, and cellular arched test model B-2 fails by web postbuckling, as can be seen from Figure 6, which confirms the identical buckling mode observed from the experimental test.

As presented in the comparative study Table 5, the load-deflection curve of Figure 7, and the failure mode shown in Figure 6, FEA modeling and analysis steps used for this investigation fairly replicate experimental test results with acceptable slight differences in stiffness due to unconsidered residual stress and real material behavior deviation from idealized bilinear stress-strain.

2.8. Parametric Investigation. After the FEA analysis results were validated in the previous section, an extensive parametric investigation was performed using the finite element package ABAQUS to evaluate the impact of arch axis and end support type on inelastic buckling performance and post-buckling mode of an arched I-section cellular steel beam under uniform distributed vertical load and mid-span concentrated load case. The test model specimens were grouped into two cases: circular axis arched cellular steel beam and parabolic arched cellular steel beam, based on arch axis geometry as depicted in Table 2. Circular axis arched cellular specimens were further clustered as a shallow arch for subtended angle $(\alpha) \leq 90^{\circ}$ and a deep arch for subtended angle $(\alpha) > 90^{\circ}$. Test model specimens of the rise-to-span ratio (H_S/L_S) in the range of 0.09–0.5 with a span length of 2.5 m modeled with the four different possible real-condition end support types presented in Table 3.

3. Results and Discussion

3.1. Impact of Arch Axis. Circular arches of subtended angles in the range of 45°–180° specimens and parabolic arched cellular beams, which have correspondingly identical span lengths of 2.5 m and an equivalent rise-to-span ratio as depicted in Table 2, were subjected to mid-span point load

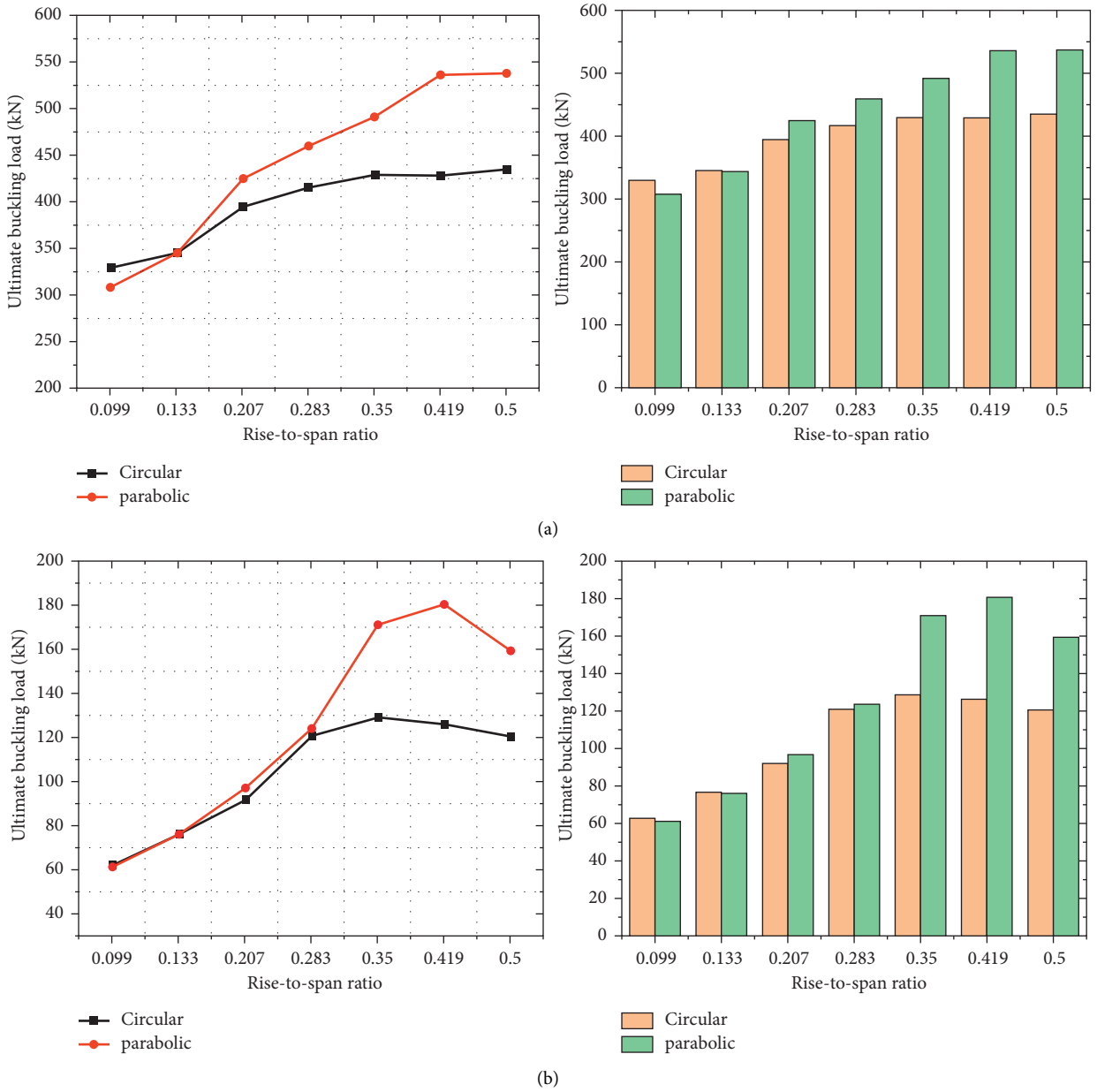

Figure 8: Impact of the arch axis on buckling performance with varying rise-to-span ratio: (a) under mid-span point load; (b) under uniform vertical distributed load.

and uniformly distributed vertical loads. As it can be seen from Figure 8(a), under mid-span point load, very shallow arch SCC-1 supports more buckling load by 6.54% than its identical PSC-1, but as the rise-to-span ratio of the arch increases, parabolic arched cellular steel becomes stiffer and supports more buckling load than the corresponding circular axis arches. Also, under uniformly distributed vertical loads, parabolic axis arched cellular beams withstand larger inelastic buckling loads than their equivalent circular axis arches as the rise-to-span ratio of the arch increases, as presented in Figure 8(b). This indicates that as the rise-to-span ratio increases, high internal axial compressive forces are generated in the parabolic axis arch of cellular steel beams when compared to a circular axis arched cellular steel beam. Because of this mechanics, parabolic axis arched cellular steel beams with a high rise-to-span ratio can support a greater inelastic buckling load than equivalent circular axis arched cellular steel beams.

3.2. Effect of End Support Condition. The arch structural member supports loads primarily by compression action. Therefore, the support stiffness has a significant influence on the in-plane strength of the arch structural member. This section discusses the effect of end support types on the in-plane strength of arched cellular steel beams. The nonlinear numerical analysis was performed on the circular and parabolic arch axis presented in Table 2 by varying end

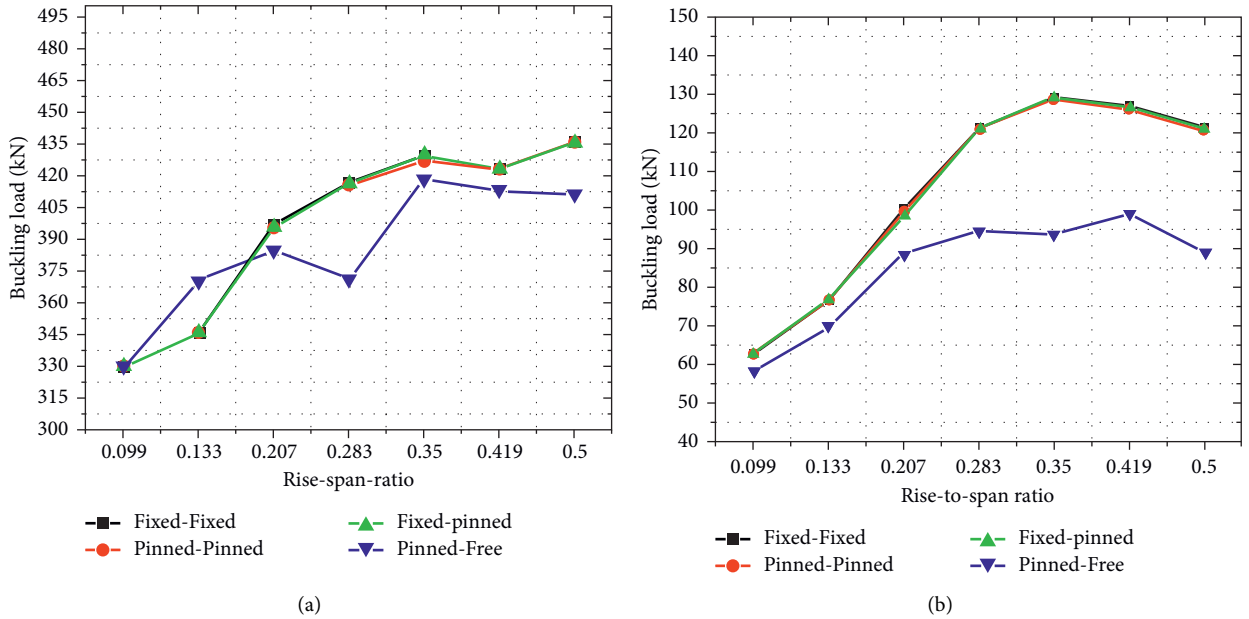

Figure 9: Effect of end support type on circular axis arched cellular steel beam: (a) under mid-span point load; (b) under uniform distributed vertical load.

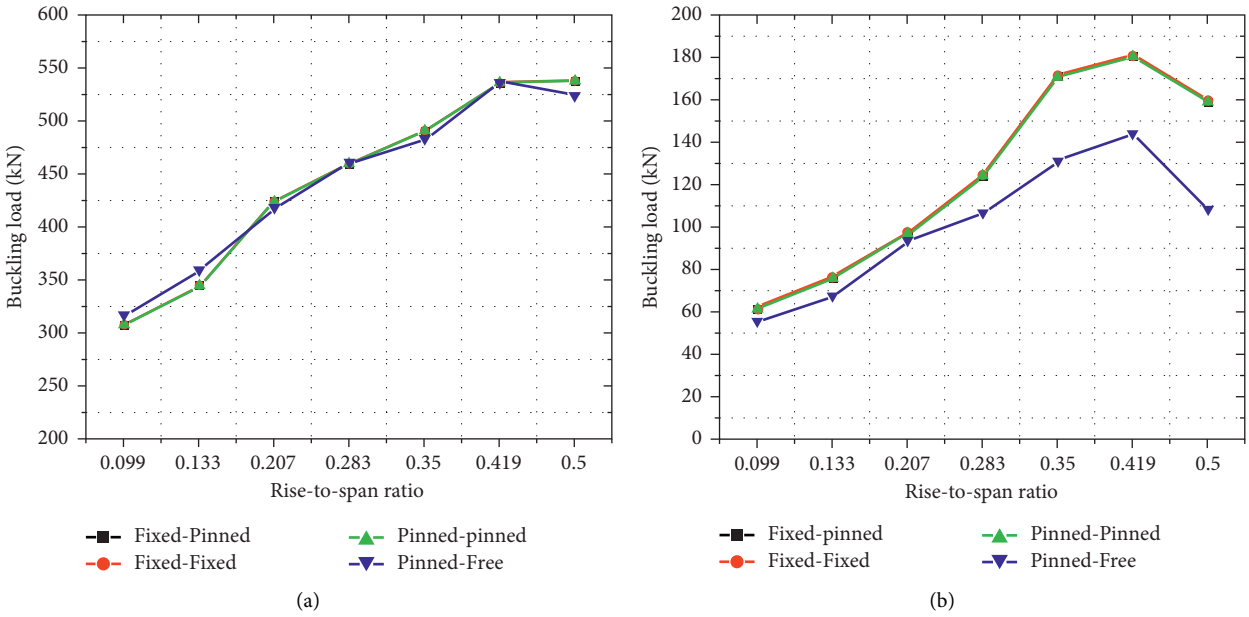

Figure 10: Effect of end support type on parabolic axis arched cellular steel beams: (a) under mid-span point load; (b) under uniform vertical load.

support configurations: pinned in-plane and free out-of-plane end supports; pinned both in-plane and out-of-the plane end supports; fixed in-plane and pinned out-of-the plane end supports; fixed in both in-plane and out-of-the plane end supports. The arrangement of the end support conditions is shown in Figure 4 and described in Table 3. From the finite element analysis, it was found that changing the end support types from pinned in both in-plane and out-of-plane to either fixed in-plane and pinned out-of-plane or fixed in both in-plane and out-of-plane has no significant impact on inelastic buckling load-carrying capacity and post-buckling modes of both circular and parabolic axis arched cellular steel beams under mid-span point load and uniform vertical load as depicted in Figures 9 and 10, respectively. This result implies that due to the occurrence of local web post-buckling failure on the web post near the loading point, end support types have no significant impact on the ultimate load-carrying capacity of circular and parabolic arched cellular steel beams under mid-span point load. However, as it can be seen from Figures 9(b) and 10(b),

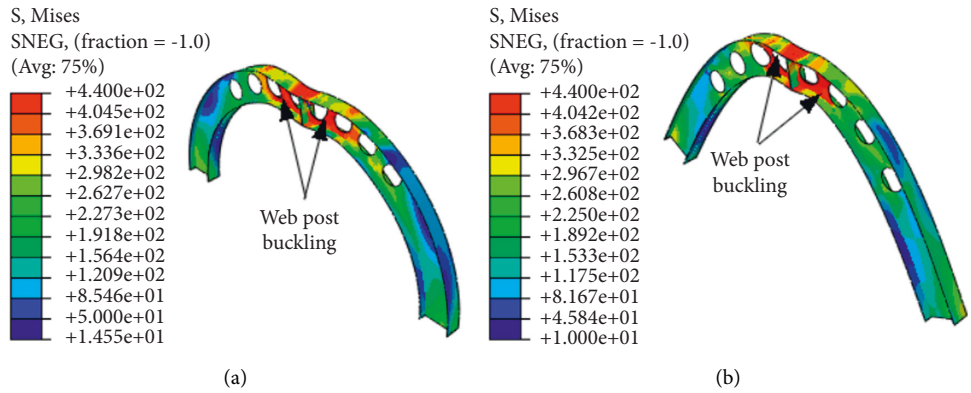

Figure 11: Web postbuckling failure mode of the circular and parabolic arched cellular steel beam: (a) DCC-4; (b) PDC-4.

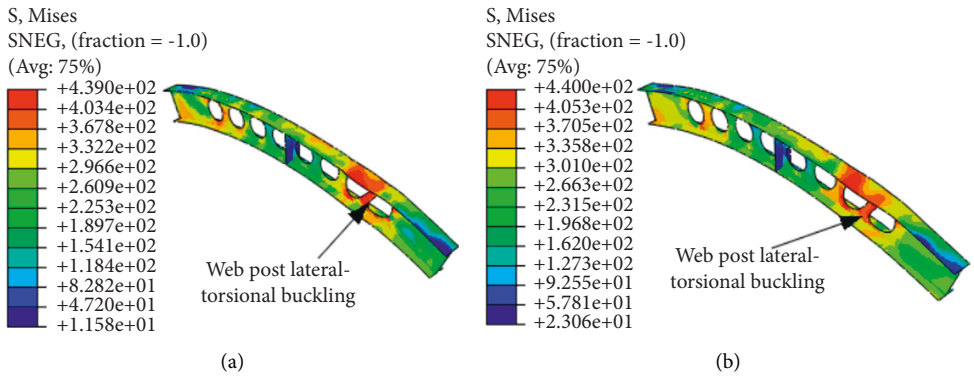

Figure 12: Web post lateral-torsional buckling of shallow cellular arch: (a) SCC-1; (b) PSC-1.

providing only pinned in-plane end support by letting the out-of-plane end free results in a reduction of the inelastic buckling strength of both circular and parabolic arched cellular steel beams under uniformly distributed vertical load. This shows that under uniformly distributed vertical load, both circular axis and parabolic axis arched cellular steel beams are subjected to lateral twisting flexure in addition to the axial compression and in-plane flexure. The lateral twisting flexure reduces the in-plane buckling strength of the arch member in addition to the axial compression and in-plane flexure. Therefore, under uniform distributed vertical load, restraining the out-of-the-plane end support enhances the ultimate buckling capacity of the arched cellular steel beam.

3.3. Buckling Mode. Mid-span point load induces combined nonuniform axial compressive and bending internal action across the span of the arch. These combined axials and bending action unevenly varied along the arch axis in the case of solid web I-section arches. Due to this uneven internal stress distribution along solid web arch length, it is difficult to predict the buckling mode of arched steel member under mid-span point load [35]. Unlike this phenomenon of the solid web, under mid-span point load, the predicted buckling mode of circular axis and parabolic axis arched cellular steel beams indicate that the failure modes observed were web postbuckling of the web post near to the applied load regardless of the variation of rise-to-span ratio in all specimens presented in Table 2. This implies that under mid-span point loads, the first two web posts near load application points are subjected to a high horizontal shear force, inducing diagonal compression stress over the web post. This compression stress twists the web post over its vertical axis, as shown in Figure 11.

Under uniform distributed vertical loads, various buckling modes were observed as the rise-to-span ratio of the arch increased. Unsymmetrical lateral-torsional web buckling was noticed on web post near to end support of one side on shallow circular and parabolic arched cellular steel beam specimens, as shown in Figure 12. As the rise-to-span ratio of specimens increases from 0.20 to 0.35 for circular and parabolic arched cellular steel beams, symmetric inelastic out-of-plane buckling is noticed in both arch axis geometry as presented in Figure 13. As the arches become very deep by increasing the rise-to-span ratio in a range of 0.42–0.5, both parabolic and circular cellular arches buckle in unsymmetrical inelastic out-of-plane mode, as can be seen from Figure 14. Generally, this indicates that uniformly distributed vertical loads induce combined nonuniform axial compressive, twisting, and bending internal action across the span of the arched

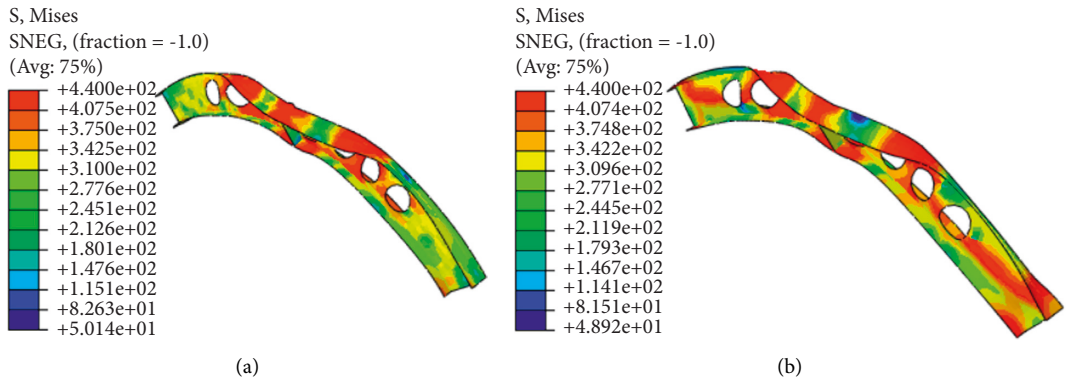

Figure 13: Symmetric out-of-plane buckling: (a) SCC-3; (b) PSC-3.

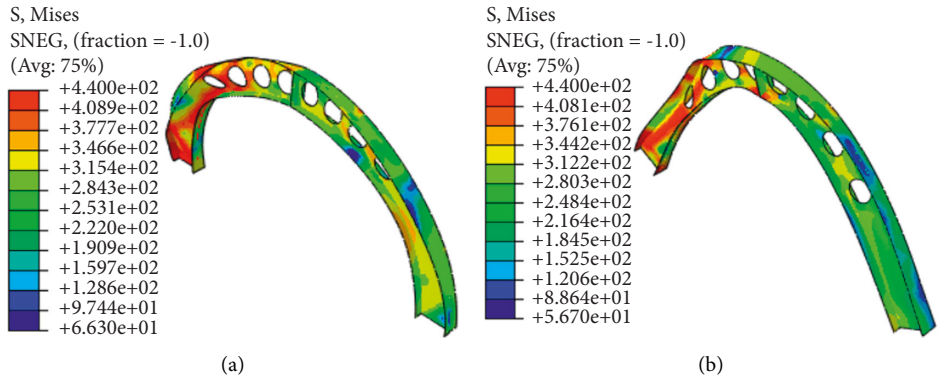

Figure 14: Unsymmetric inelastic buckling mode of deep cellular arch: (a) DCC-4; (b) PDC-4.

cellular steel beams. These combined axial, twisting, and bending actions were unevenly varied along the arch axis with the rise-to-span ratio of the arched cellular steel beams. Due to this, under uniform distributed vertical loads, circular and parabolic arched cellular steel beams of the same span length of different rise-to-span ratios may buckle in different modes. Further, the predicted failure mode shows that under uniform distributed vertical load, the rise-to-span ratio has a significant influence on the internal stress distribution of and buckling modes of arched cellular steel beams.

4. Conclusions

In this study, the effect of arch axis geometry and impact of end support types on ultimate inelastic buckling strength and post-buckling mode of arched cellular steel beams under uniform distributed vertical load and mid-span concentrated load was investigated using the nonlinear finite element analysis package ABAQUS. Material nonlinearity, a second-order effect due to large deformation, and initial geometric imperfection were contemplated in the nonlinear analysis of the test specimens. Further, the reliability of finite element analysis results was validated by comparing them to the related existing experimental work. Generally, from this study, the following conclusions were presented, but caution must be taken in applying these conclusions to uneven load distribution, opening diameter, and an unsymmetrical section of arched cellular steel beams.

(i) The FEA package ABAQUS with modeling and analyzing steps used in this investigation is capable of fairly replicating experimental work on predicting the inelastic ultimate buckling load, deflection, and buckling mode of arched cellular steel beams.

(ii) When subjected to a uniform distributed vertical load and a mid-span concentrated load, shallow circular axis arched SCC-1 of the rise-to-span ratio of 0.09, and a subtended angle of 45^0, the circular axis arched cellular beam supports greater inelastic buckling load by 2.13% and 6.55%, respectively, when compared to a parabolic axis arched cellular steel beam of the same rise-to-span ratio and span length. But, as the rise-to-span ratio increases beyond 0.13, parabolic axes, arched cellular steel beams become stiffer and more structurally efficient than their equivalent circular axis arched cellular steel beams.

(iii) The arch axis geometry (circular and parabolic) has no significant impact on the buckling mode of arched cellular steel beams.

(iv) Under uniform radially distributed vertical loads, the inelastic buckling mode of arched cellular steel

beams is significantly dependent on the rise-to-span ratio of the arch.

(v) Except for in-plane pinned and free out-of-plane end support conditions, altering the end support type from both in-plane and out-of-plane pinned end to either in-plane fixed and out-of-plane pinned end or both in-plane and out-of-plane fixed ends has no considerable impact on inelastic ultimate buckling strength and buckling mode under mid-span point load and uniformly distributed vertical load.

(vi) From the test sample analysis, pinned in-plane and free out-of-plane end support types yield reduced inelastic ultimate buckling load-carrying capacity of both circular and parabolic arched cellular steel beams under uniformly distributed vertical load when compared to other possible end support types of the steel arch member.

Data Availability

The modeling and analysis data results from numerical simulation included within the article and extra data required to support the findings are available from the author upon request.

Conflicts of Interest

The author declares that there are no conflicts of interest regarding the publication of this article.

References

[1] ArcelorMittal, "The Intelligent Solution for Long Spans," 2011, http://www.constructalia.com/english/publications/brochures/acb_cellular_beams#.V6uADCh96Uk.

[2] S. S. Fares, J. Coulson, and D. W. Dinehart, *Castellated and Cellular Beam Design. Steel Design Guide 31*, Am. Inst. Steel Constr, Washington, DC, 2016.

[3] P. D. Pachpor, N. D. Mittal, L. N. Gupta, and N. V. Deshpande, "Finite element analysis and comparison of castellated and cellular beam," *Advanced Materials Research*, vol. 264–265, pp. 694–699, 2011.

[4] M. Trading, *Cellular Beams Design Guide*, South Africa, Johannesburg, 2003.

[5] D. Kerdal and D. a. Nethercot, "Failure modes for castellated beams," *Journal of Constructional Steel Research*, vol. 4, pp. 295–315, 1984.

[6] P. Panedpojaman and T. Rongram, "Design equations for Vierendeel bending of steel beams with circular web openings," *Proc. World Congr*, pp. 1493–1498, London, U.K, 2014.

[7] K. F. Chung, C. H. Liu, and A. C. H. Ko, "Steel beams with large web openings of various shapes and sizes: an empirical design method using a generalised moment-shear interaction curve," *Journal of Constructional Steel Research*, vol. 59, no. 9, pp. 1177–1200, 2003.

[8] K. F. Chung, T. C. H. Liu, and A. C. H. Ko, "Investigation on vierendeel mechanism in steel beams with circular web openings," *Journal of Constructional Steel Research*, vol. 57, no. 5, pp. 467–490, 2001.

[9] S. Durif, A. Bouchaïr, and O. Vassart, "Experimental tests and numerical modeling of cellular beams with sinusoidal openings," *Journal of Constructional Steel Research*, vol. 82, pp. 72–87, 2013.

[10] L. F. Grilo, R. H. Fakury, A. L. R. d. Castro e Silva, and G. d. S. Veríssimo, "Design procedure for the web-post buckling of steel cellular beams," *Journal of Constructional Steel Research*, vol. 148, pp. 525–541, 2018.

[11] P. Panedpojaman, "Buckling analysis for web post of cellular beams," *10th Int. PSU Eng. Conf. May*, vol. 53, 2012.

[12] R. M. Lawson, J. Lim, S. J. Hicks, and W. I. Simms, "Design of composite asymmetric cellular beams and beams with large web openings," *Journal of Constructional Steel Research*, vol. 62, no. 6, pp. 614–629, 2006.

[13] P. Panedpojaman, T. Thepchatri, and S. Limkatanyu, "Thin-Walled Structures Novel design equations for shear strength of local web-post buckling in cellular beams," in *Thin Walled Struct*, pp. 92–104, Elsevier, Amsterdam, Netherlands, 2014.

[14] F. Erdal and M. P. Saka, "Ultimate load carrying capacity of optimally designed steel cellular beams," *Journal of Constructional Steel Research*, vol. 80, pp. 355–368, 2013.

[15] F. P. V. Ferreira and C. H. Martins, "LRFD for lateral-torsional buckling resistance of cellular beams," *International Journal of Civil Engineering*, vol. 18, no. 3, pp. 303–323, 2020.

[16] M. Hosseinpour and Y. Sharifi, "Finite element modelling of castellated steel beams under lateral-distortional buckling mode," *Structures*, vol. 29, pp. 1507–1521, 2021.

[17] Y. L. Pi and M. A. Bradford, "Nonlinear elastic analysis and buckling of pinned-fixed arches," *International Journal of Mechanical Sciences*, vol. 68, pp. 212–223, 2013.

[18] Y. L. Pi, M. A. Bradford, and B. Uy, "In-plane stability of arches," *International Journal of Solids and Structures*, vol. 39, no. 1, pp. 105–125, 2002.

[19] Y. L. Pi and M. A. Bradford, "Non-linear buckling and postbuckling analysis of arches with unequal rotational end restraints under a central concentrated load," *International Journal of Solids and Structures*, vol. 49, no. 26, pp. 3762–3773, 2012.

[20] C. Dou, Y.-L. Guo, S.-Y. Zhao, and Y.-L. Pi, "Experimental investigation into flexural-torsional ultimate resistance of steel circular arches," *Journal of Structural Engineering*, vol. 141, no. 10, Article ID 04015006, 2015.

[21] C. F. Hu, Y. L. Pi, W. Gao, and L. Li, "In-plane non-linear elastic stability of parabolic arches with different rise-to-span ratios," *Thin-Walled Structures*, vol. 129, pp. 74–84, 2018.

[22] Z. Tang, W. Zhang, J. Yu, and S. Pospíšil, "Prediction of the elastoplastic in-plane buckling of parabolic steel arch bridges," *Journal of Constructional Steel Research*, vol. 168, p. 105988, 2020.

[23] Y. L. Pi and N. S. Trahair, "Closure to "out-of-plane inelastic buckling and strength of steel arches" by yong-Li Pi and N. S. Trahair," *Journal of Structural Engineering*, vol. 124, pp. 352-353, 1997.

[24] Y. L. Pi and M. A. Bradford, "In-plane strength and design of fixed steel I-section arches," *Engineering Structures*, vol. 26, no. 3, pp. 291–301, 2004.

[25] Y. L. Guo, S. Y. Zhao, Y. L. Pi, M. A. Bradford, and C. Dou, "An experimental study on out-of-plane inelastic buckling strength of fixed steel arches," *Engineering Structures*, vol. 98, pp. 118–127, 2015.

[26] O. F. Zaher, N. M. Yossef, M. H. El-Boghdadi, and M. A. Dabaon, "Structural behaviour of arched steel beams with cellular openings," *Journal of Constructional Steel Research*, vol. 148, pp. 756–767, 2018.

[27] S. Pandya and M. Dhankot, "FE Analysis of Curved Castellated Girder for Variable Thermal Condition," *Kalpa Publications in Civil Engineering*, vol. 1, pp. 192–185, 2018.
[28] Eurocode 3, *Design of Steel Structures: Part 1-1, General Rules and Rules for Building*, British Standards Institution, BS EN, London, UK, 2005.
[29] B. Dowswell, "Curved Member Design Design Guide," vol. 33American Institute of Steel Construction, Chicago, 2018.
[30] Dassault Systèmes Simulia Corp, *ABAQUS 6.13 Theory Guide*, Dassault Systèmes Simulia Corp, Providence, RI, USA, 2013.
[31] B. A. Memon and X. Z. Su, "Arc-length technique for nonlinear finite element analysis," *Journal of Zhejiang University - Science*, vol. 5, pp. 618–628, 2004.
[32] N. M. Lafontaine, X. R. Wang, K. F. Huang, M. W. Yuan, and E. Oñate, *On the Arc Length Method: Combining Ideas and Implementations Aspects*, NY City, 2013.
[33] R. C. Spoorenberg, H. H. Snijder, J. C. D. Hoenderkamp, and D. Beg, "Design rules for out-of-plane stability of roller bent steel arches with FEM," *Journal of Constructional Steel Research*, vol. 79, pp. 9–21, 2012.
[34] R. C. Spoorenberg, *Structural Properties and Out-Of-Plane Stability of Roller Bent Steel Arches*, 2011.
[35] A. Liu, H. Lu, J. Fu, and Y. L. Pi, "Lateral-torsional buckling of fixed circular arches having a thin-walled section under a central concentrated load," *Thin-Walled Structures*, vol. 118, pp. 46–55, 2017.